[Supporting Information to accompany]

J-aggregation Induced Low Bandgap Anthracene-based Conjugated Molecule for Solution-processed Solar Cells

Jicheol Shin,[a] Nam Su Kang.[bc] Kyung Hwan Kim,[a] Tae Wan Lee,[a] Jung-Il Jin,[a] Minsik Kim,[a] Kwangyeol Lee,[a] Byeong Kwon Ju,[b] Jae-Min Hong,[c] and Dong Hoon Choi[a]*

[a]*Department of Chemistry, Research Institute for Natural Sciences, Korea University, 5 Anam-dong, Sungbik-gu, Seoul 136-701, Republic of Korea.*

[b] *Display and Nanosystem Laboratory, College of Engineering Korea University, Seoul 136-701, Republic of Korea*

[c]*Future Convergence Research Division, Korea Institute of Science and Technology(KIST), 14-5 Hwarang-ro, Seoul 136-791, Republic of Korea*

* To whom correspondence should be addressed. E-mail: dhchoi8803@korea.ac.kr

1. Instrumentation: ^{1}H NMR spectra were recorded on a Varian Mercury NMR 400Hz spectrometer using deuterated chloroform purchased from Cambridge Isotope Laboratories, Inc. ^{13}C NMR spectra were recorded using a Varian Inova-500 spectrometer. Elemental analyses were performed using an EA1112 (Thermo Electron Corp.) elemental analyzer. High resolution mass analysis was performed on a JMS-700 MStation mass spectrometer (JEOL, resolution 60,000, m/z range at full sensitivity 2,400). Thermal properties were studied under a nitrogen atmosphere on a Mettler DSC 821^{e} instrument. Thermal gravimetric analysis (TGA) was conducted on a Mettler TGA50 (temperature rate 10 ^{o}C/min under N_2).

The redox properties of the molecule were examined by using cyclic voltammetry (Model: EA161 eDAQ). Thin films were coated on a platinum plate using chloroform as a solvent. The electrolyte solution employed was 0.10 M tetrabutylammonium hexafluorophosphate (Bu_4NPF_6) in a freshly dried acetonitrile. The Ag/AgCl and Pt wire (0.5 mm in diameter) electrodes were utilized as reference and counter electrodes, respectively. The scan rate was at 50 mV/s.

Atomic force microscopy (AFM, Advanced Scanning Probe Microscope, XE-100, PSIA) operating in tapping mode with a silicon cantilever was used to characterize the surface morphologies of the thin films. The film sample was fabricated by spin-coating the chloroform solution on n-octyltrichlorosilane (OTS)-treated silicon wafer followed by drying at 50 ^{o}C under vacuum (solvent: chloroform, conc. of the solution: 10 mg/mL). The AFM images of the blend films for OPV were obtained from the thin films fabricated by spin-coating the chlorobenzene solution on PEDOT:PSS layer on ITO glass.

In order to study absorption and emission behaviors, thin films were fabricated on quartz substrates as follows. A chloroform solution (1 wt%) was filtered through an acrodisc syringe filter (Millipore 0.45 μm, Billerica, MA, USA) and subsequently spin-cast on quartz glass. The films were dried overnight at 60 ^{o}C for 12 hr under vacuum. Absorption spectra of the samples as films and as a solution (chloroform, concentration 1 x 10^{-6} mole L^{-1}) were

obtained using a UV-Vis spectrometer (HP 8453, photodiode array type) in the wavelength range 190-1100 nm. Photoluminescence spectroscopy was performed by using Hitachi F-7000 fluorescence spectrophotometer.

XRD measurements were performed with a Rigaku D/MAX Ultimata 3. The measurements were recorded over a range of 2° < 2θ□< 45° and X'celerator detector operating at 40 kV and 30 mA. The film samples were fabricated by spin coating the solution on a silicon wafer followed by drying at 50°C under vacuum (solvent: chlorobenzene, conc. of the solution: 10 mg/mL). Scanning electron microscopy (SEM) image of the **HBTATHT** crystal microplatelet was obtained using a Jeol JSM-7500F. All transmission electron microscopy (TEM) images of the blend films with **HBTATHT** and PCBM were obtained at 200 keV with LaB6 filament, using a Tecnai G2 F20 S-Twin and recorded with a 2K x 2K pixel resolution Veleta TEM camera (Olympus) on Cu TEM grids. Thin active-layer (~100 nm) films were spin-cast on the surface of PEDOT:PSS coated on ITO. Active layers were immersed in deionized water (5 min) and floated onto the air/water interface. Small sized films were picked up on unsupported 200 mesh copper grids.

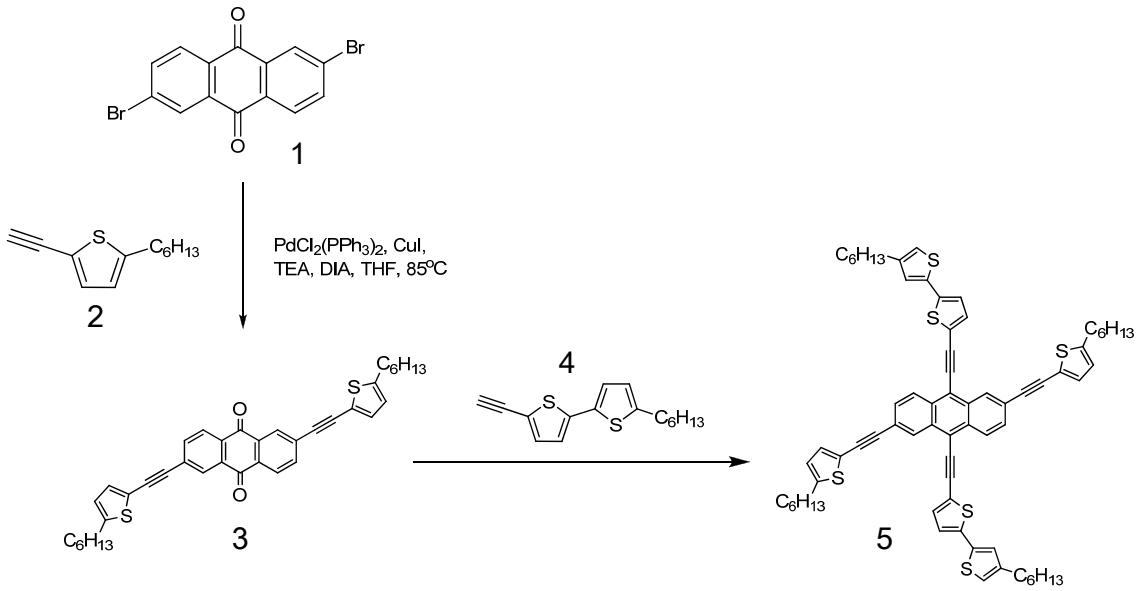

Scheme 1S. Synthetic procedure for **HBTATHT**.

2. Synthesis

Materials All chemicals were obtained from commercial sources and used without further purification. All of the reactions and manipulations carried out under N_2 with the use of standard inert-atmosphere and Schlenk techniques unless otherwise noted. Solvent used in inert-atmosphere reactions were dried and degassed using standard procedures. All deuterated solvent were purchased from Cambridge Isotope Laboratories, Inc.

2,6-Dibromoanthracene-9,10-dione (1), 2-ethynyl-5-hexylthiophene (2), 2,6-bis((5-hexylthiophen-2-yl)ethynyl)anthracene-9,10-dione (3), and 5-ethynyl-5'-hexyl-2,2'-bithiophene (4) were synthesized by following our previous literature methods.[S1-S7]

5',5''-(2,6-Bis((5-hexylthiophen-2-yl)ethynyl)anthracene-9,10-diyl)bis(ethyne-2,1-diyl)bis(4-hexyl-2,2'-bithiophene) (5): 5-Ethynyl-5'-hexyl-2,2'-bithiophene, **4** (1.39 g, 5.1 mmol) was dissolved in freshly distilled tetrahydrofuran (100 mL) in a 250 mL, oven dried, mag.-stirred round bottom flask. The solution was then cooled to –78°C. n-BuLi (2.0 mL, 5.1 mmol, 2.5 M solution. in hexane) was then added dropwise over 5 minutes. The mixture was stirred for 30 min, and 2,6-bis((5-hexylthiophen-2-yl)ethynyl)anthracene-9,10-dione, 3 (1 g, 1.7 mmol) was added at -78 °C. The mixture was allowed to stir at room temperature for 3 hours, and then quenched with water, $SnCl_2$, and HCl. After completing the reaction, the solution was poured into methanol to collect the precipitates. The crude solid was purified by recrystallization in methanol. Yield 1.0 g, 56 %. ^{1}H-NMR (400 MHz, $CDCl_3$): δ(ppm) 8.60 (s, 2H), 8.42 (d, J = 8.6 Hz, 2H), 7.61 (d, J = 8.2 Hz, 4H), 7.40 (d, J =9.0 Hz, 2H), 7.21 (d, J = 8.2 Hz, 4H), 7.07 (d, J = 3.5 Hz, 2H), 6.72 (d, J = 3.5 Hz, 2H), 2.82 (t, 4H), 2.80 (t, 4H), 1.74-1.67 (m, 8H), 1.39-1.32 (m, 24H), 0.91 (t, 12H). ^{13}C NMR (100 MHz, $CDCl_3$): δ(ppm) 149.18, 146.68, 140.83, 134.31, 133.82, 132.79, 131.45, 130.46, 129.62, 125.24, 124.60, 124.43, 123.28, 122.81, 122.06, 121.39, 121.03, 120.61, 118.02, 96.89, 93.37, 91.22, 85.94, 31.81, 30.54, 30.48, 29.02, 22.82, 14.34. HR-MS (EI) m/z $[M]^+$: Calcd for $C_{70}H_{70}S_6$, 1103.69; found, 1103.39. Anal. Calcd. for $C_{70}H_{70}S_6$: C, 76.18 ; H, 6.39 ; S, 17.43 found : C, 76.15 ; H, 6.41 ; S, 17.44.

3. OFET device fabrication: For the characterization of TFT performance, bottom gate top contact device geometry was employed. On the heavily n-doped SiO_2/Si substrate the spin-coated films (thickness ~50-60 nm) of **HBTATHT** were prepared with chloroform as a solvent. Surface modification was carried out with OTS to make hydrophobic dielectric surface. Source and drain electrodes were then thermally evaporated (100 nm) through shadow mask with channel width and length of 1500 μm, and 100 μm, for TFT devices respectively. To characterize the single-crystal microplatelet FET performance, a bottom-gate top-contact device geometry was also employed. **HBTATHT** was dissolved in THF, respectively and slow diffusion method over methanol was employed to grow high quality crystalline microplatelets on the surface of OTS-treated SiO_2 insulator. All the field effect mobilities were extracted in the saturation regime using the relationship $\mu_{sat}=(2I_{DS}L)/(WC(V_G-V_{th})^2)$, where I_{DS} means saturation drain current, C is capacitance of SiO_2 dielectric, V_G is gate bias, and V_{th} is threshold voltage. The device performance was evaluated in air using 4200-SCS semiconductor characterization system.

4. OPV device fabrication

The hole collecting electrode was 150 nm thick indium tin oxide (ITO) coated glass with resistance of 15.0 Ω / cm. ITO glass was cleaned by sonication in the mixture of isopropyl alcohol and acetone (50:50), chloroform, and isopropyl alcohol for 30 minutes in each solvent. And, the cleaned ITO coated glass was treated with O_2 plasma and flattening ITO with a microwave-generated plasma reactor (CR403M, 90 W) for 10 minutes. 50 nm thick PEDOT:PSS layer (Baytron P, 1 S cm^{-1}) was coated by spin coating stock solution at 4000 rpm for 40 seconds. PEDOT:PSS coating was thermally treated in the glove box at 100 ^{o}C for 30 minutes.

The molecules, **HBTATHT** and $PC_{61}BM$ (or $PC_{71}BM$) were dissolved in anhydrous chlorobenzene. The solution was spin coated on PEDOT:PSS layer and the active layer (100 nm) was dried under vacuum at 60 ^{o}C for 6 hr. 150 nm thick aluminum was evaporated on LiF thin layer as an electrode. Current-voltage characteristics were measures with Keithley 2400 source-measure unit. 300 W Xe lamp was used as a light source to produce intensity of 100 mW cm^{-2}. To mimic sun light, AM 1.5 filter (Oriel) was used neutral density filter was used to reduce intensity as necessary. Intensity of incoming light power was measured with calibrated broadband optical power meter (Spectra Physics model 404).

5. Thermal analysis

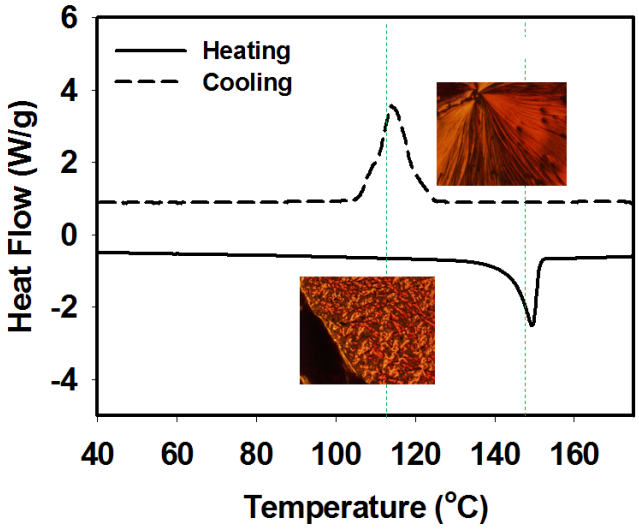

Figure 1S. DSC thermogram of **HBTATHT**. *inset: crystalline phase images

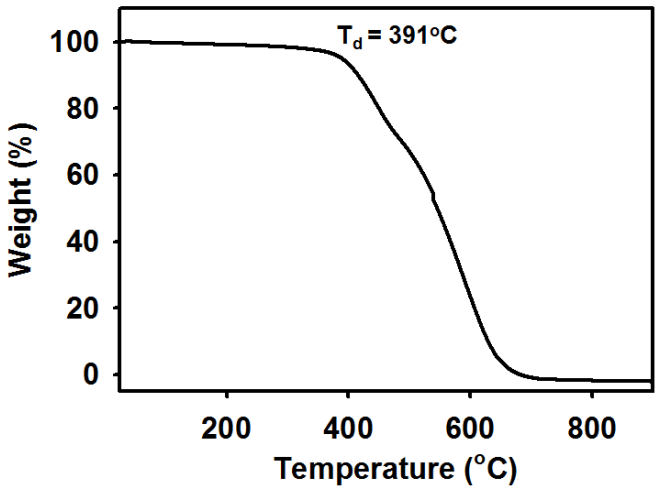

Figure 2S. TGA thermogram of **HBTATHT**.

Thermal decomposition temperature was monitored in TGA thermogram, which was found to be around 391 ^{o}C. DSC measurement was performed at a heating (cooling) scan rate of 10 (-10) ^{o}C/min under nitrogen, with the highest temperature limited to a value below the

decomposition temperature. The **HBTATHT** molecule exhibited distinct crystalline-isotropic transition temperature and cold crystallization temperature of 149 °C and 114 °C, respectively.

6. Comparison of absorption and cyclic voltammograms of two similar compounds.

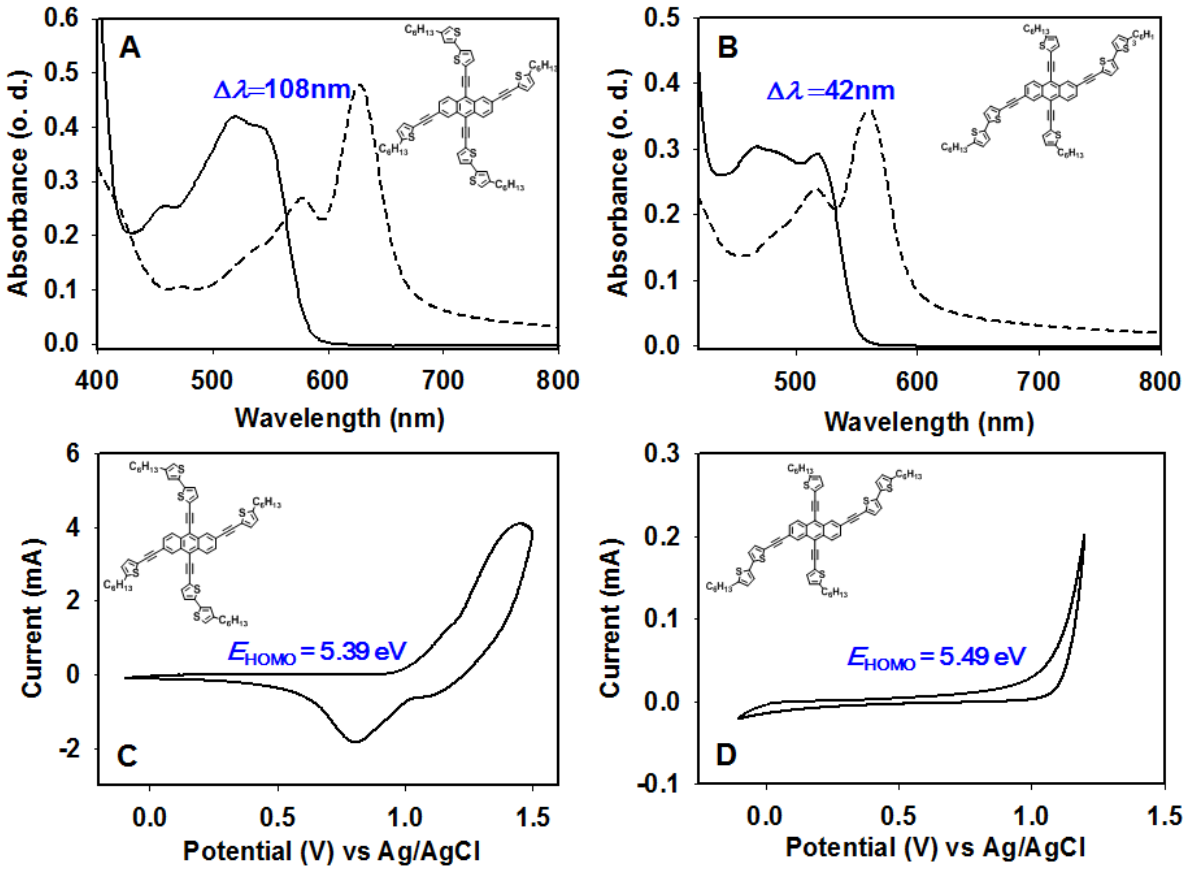

Figure 3S. Absorption spectra of solution and film samples. (A) **HBTATHT**, (B) HTATHBT; Cyclic voltammograms of film samples. (C) **HBTATHT**, (D) HTATHBT

7. Density functional theory (DFT) calculation

To estimate the position and molecular energies of frontier orbitals for **HBTATHT**, Density Functional Theory (DFT) calculations were performed using the Spartan'10 program at the B3LYP/6-31G* level. The hexyl peripheral groups were sustained in calculation to observe the effect of substituents on the optimized geometry and theoretical energy levels. As shown in Figure 4S, the largest coefficients in the HOMO orbitals are located on the 2-D π-system centered at an anthracene unit. The coefficients in the LUMO orbital are mainly located on the anthracene unit along 9,10-substituted positions only. It shows that the planarity of conjugated unit was sustained with a small degree of disorder around the hexyl substituents. Because of highly π-extended conjugated structure along the bithiophene (BT) units, **HBTATHT** shows a small calculated bandgap energy of 2.08 eV.

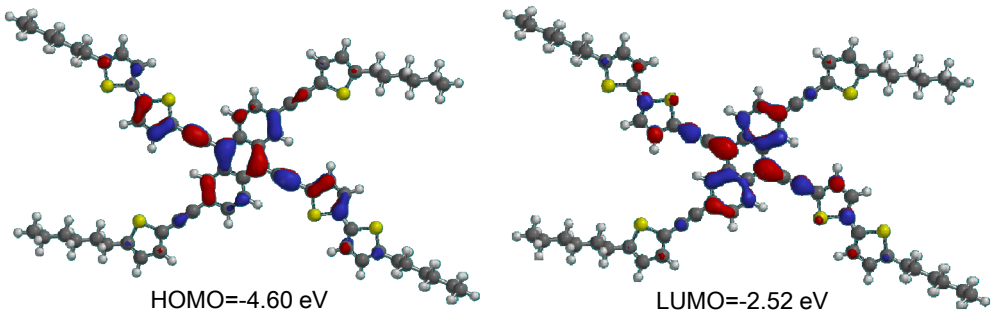

Figure 4S. HOMO/LUMO levels of **HBTATHT** used to calculate the theoretical molecular orbitals.

8. Electrochemical analysis: Cyclic voltammetry

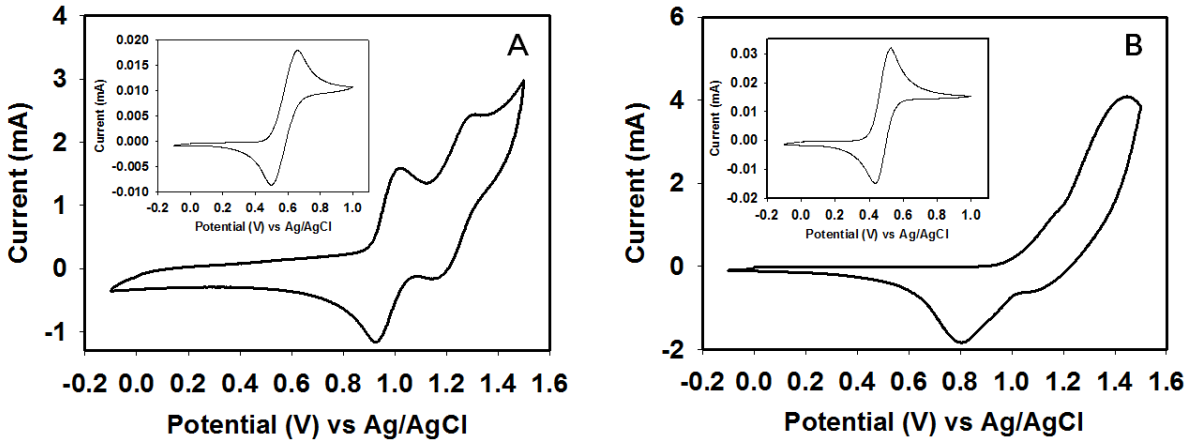

Figure 5S. Cyclic voltammograms of **HBTATHT**. *sample: solution (A), film (B). *Insets : CVs of ferrocene standard.

9. Absorption spectral analysis with the composition of J-aggregated molecules and $PC_{61}BM$.

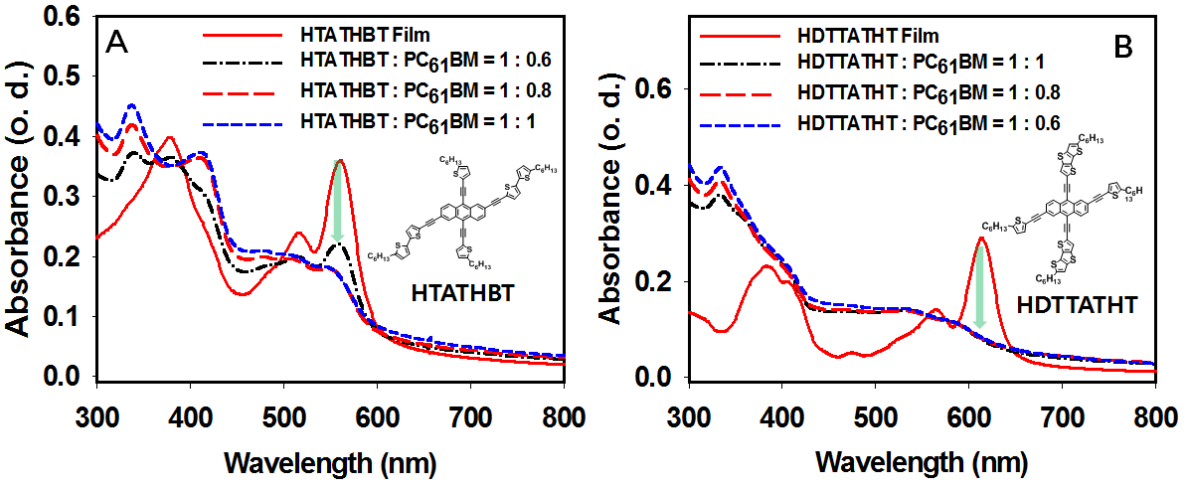

Figure 6S. A: Absorption spectra of HTATHBT and its blend films with $PC_{61}BM$. B: Absorption spectra of HDTTATHT and its blend films with $PC_{61}BM$.

The compound, HTATHBT bearing 5-ethynyl-5'-hexyl-2,2'-bithiophene at 2,6-positions was mixed with $PC_{61}BM$ with the composition. As the concentration increased, the absorbance at

562 nm decreased, which indicates the disruption of J-aggregated crystalline structure. (Figure 6S (A)), It was found that the power conversion efficiency of the BHJ sample made of HTATHBT and PCBM (1:1) only exhibited less than 0.5%.

In Figure 6S (B), the absorbance at 615 nm almost disappeared when adding $PC_{61}BM$ to HDTTATHT. The BHJ made of HDTTATHT and $PC_{61}BM$ (1:1 wt%) also exhibited very low power conversion efficiency of around 0.2 %. In brief, only by observing the persistency of the J-aggregation band in corresponding BHJ, we can anticipate whether the blend sample can show high or low PCE values in OPVs.

10. XRD analysis of HBTATHT and its blend samples with PCBM

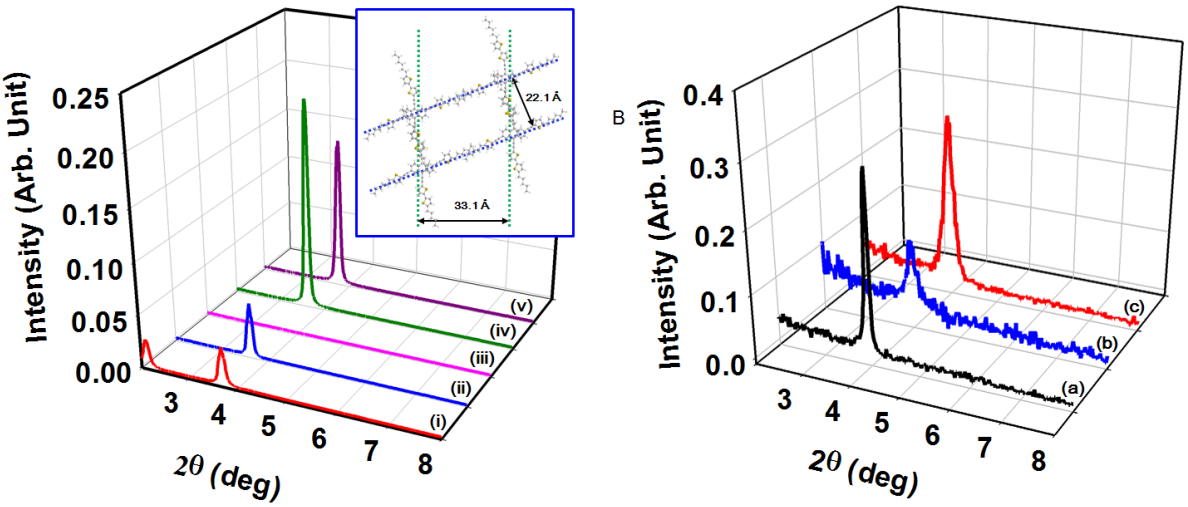

Figure 7S. A: XRD analysis of **HBTATHT** thin film with the temperature. (i) 25 ^{o}C, (ii) 100 ^{o}C, (iii) 155 ^{o}C, (iv) 113 ^{o}C (cooling cycle), (v) 25 ^{o}C (cooling cycle). *inset: the expected molecular packing geometry of **HBTATHT** molecules. B: Comparison of XRD patterns. (a) **HBTATHT** pristine film, (b) **HBTATHT**:$PC_{61}BM$=1:0.8 (wt. ratio), (c)

HBTATHT:$PC_{71}BM$= 1:0.6 (wt. ratio). The first-order diffraction peaks in (a), (b), and (c) did not change at all.

11. Electrical characteristics of thin film transistor device

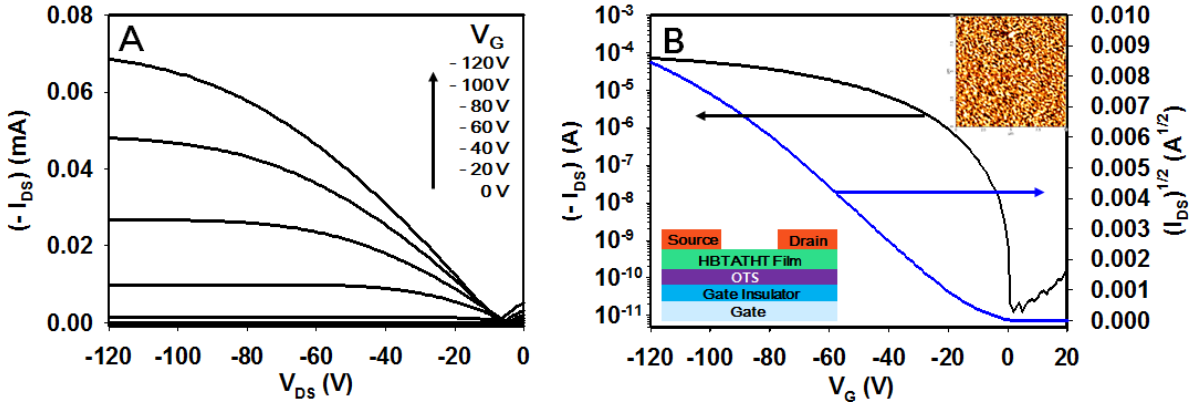

Figure 8S. (A) Output and (B) transfer curves of a TFT device made of **HBTATHT**. *Insulator: n-octyltrichlorosilane (OTS)-treated SiO_2 *Inset: atomic force microscopy (AFM) images of the pristine film in a TFT device and TFT device configuration.

12. Electrical characteristics of single-crystal FET device

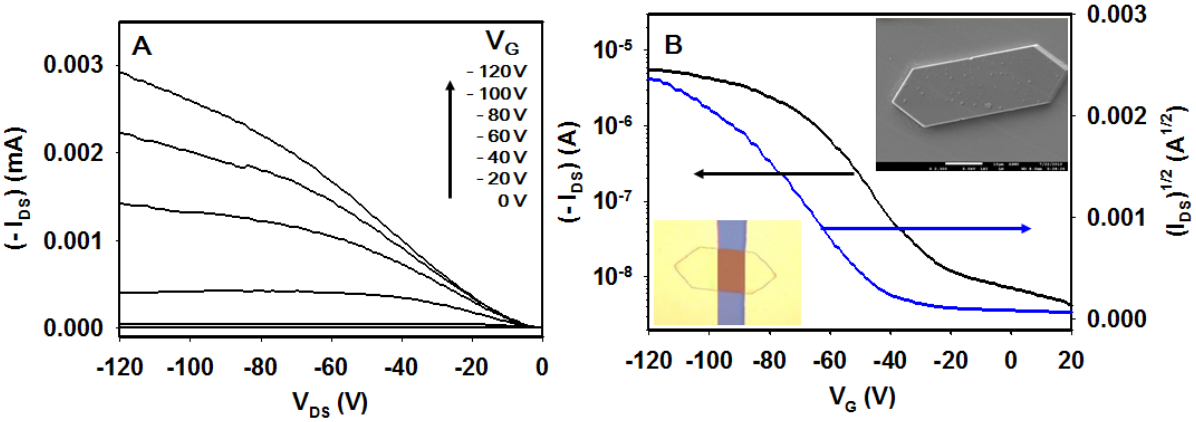

Figure 9S. Electrical characterization of a crystalline microplate FET. Output (A) and transfer (B) curves (V_{DS} = –80 V) of FET device made of **HBTATHT** Crystal. *Inset: SEM image of the crystal and optical microscopic image of FET device. L= 100 μm, W = 146.88 μm.

13. Energy level diagram

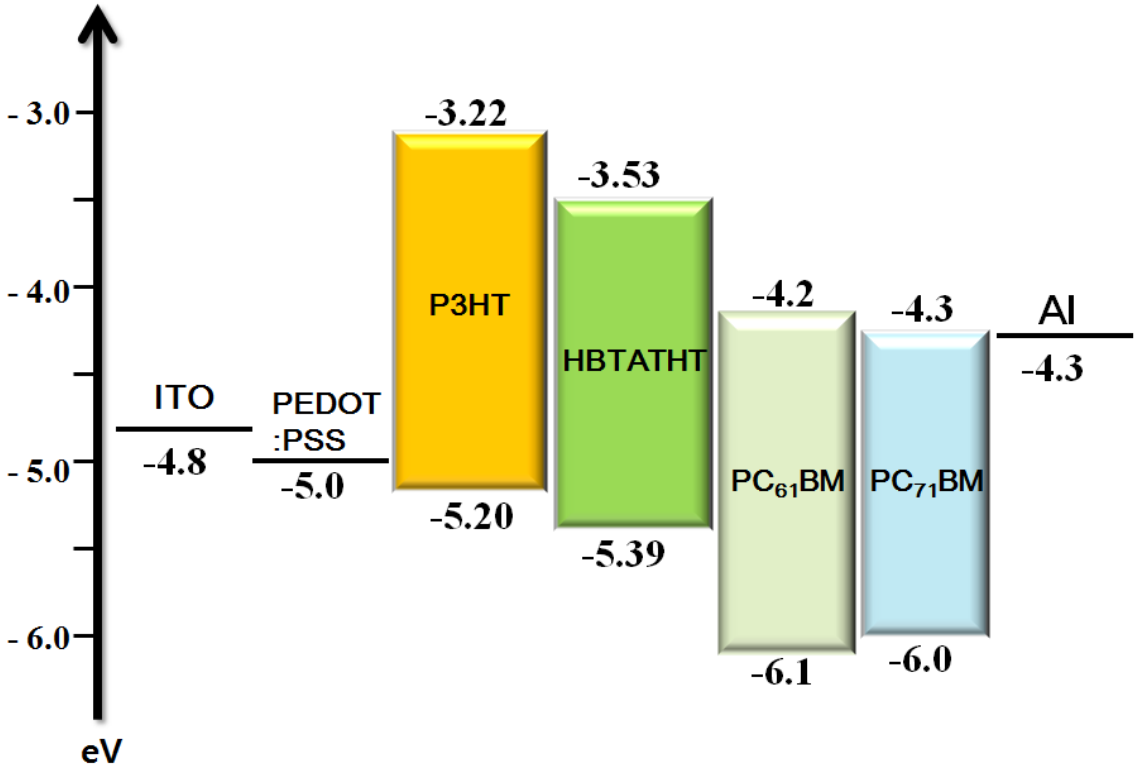

Figure 10S. Energy level alignment of P3HT, **HBTATHT**, $PC_{61}BM$, and $PC_{71}BM$ in OPV device.

14. Current density vs. voltage curves of BHJ PV devices made of HBTATHT and $PC_{61}BM$ with the composition and the IPCE spectra of OPV devices

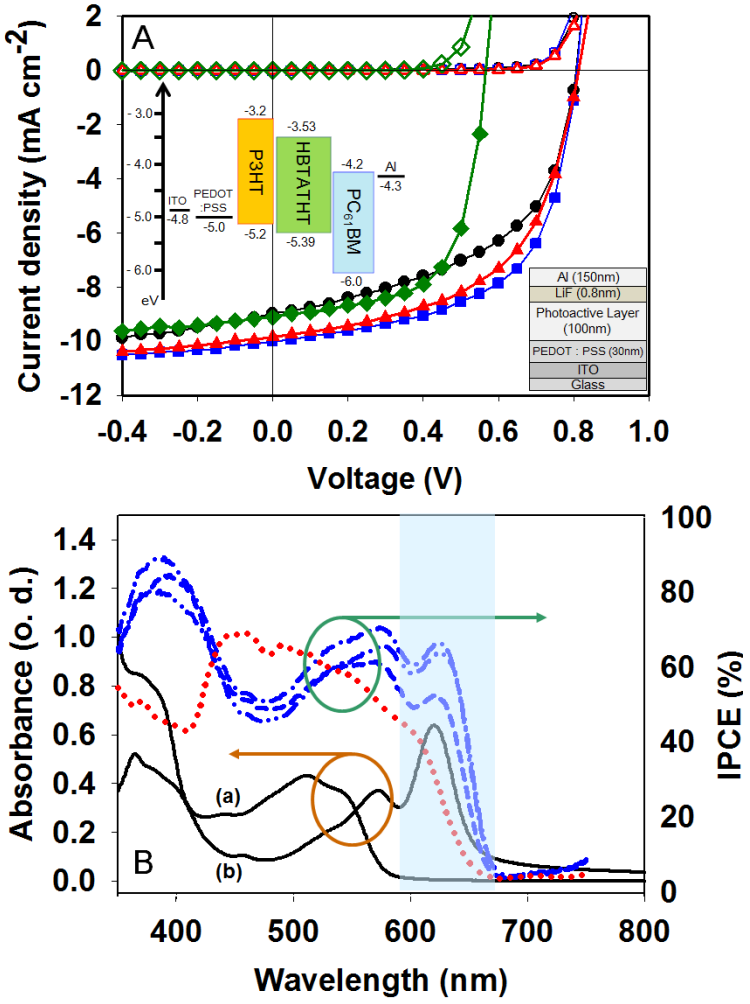

Figure 11S. (A) Current density-Voltage (*J-V*) characteristics of OPVs based on **HBTATHT** : $PC_{61}BM$ active layer with various blend compositions. *open symbols: dark current, filled symbols: photocurrent under AM 1.5 white light illumination at 100 mW cm^{-2}, *circle (1:1), square (1:0.8), triangle (1:0.6), diamond (P3HT:$PC_{61}BM$=1:0.6) (B) External quantum efficiency (EQE) of OPV cells with **HBTATHT** : $PC_{61}BM$ active layer with different blend composition. *Medium dashed line (1:1), Dash-dot-dashed line (1:0.8), Dash-dot-dot-dashed line (1:0.6), dotted line (P3HT:$PC_{61}BM$=1:0.6). *The absorption spectra of **HBTATHT** were superimposed. (a) solution, (b) film. *The shaded area denotes enhancement of absorption and EQE due to J-aggregation of **HBTATHT** compared to those of P3HT/$PC_{61}BM$ system.

15. Current density vs. voltage curves of BHJ PV devices made of HBTATHT and $PC_{71}BM$ with the composition and the IPCE spectra of OPV devices

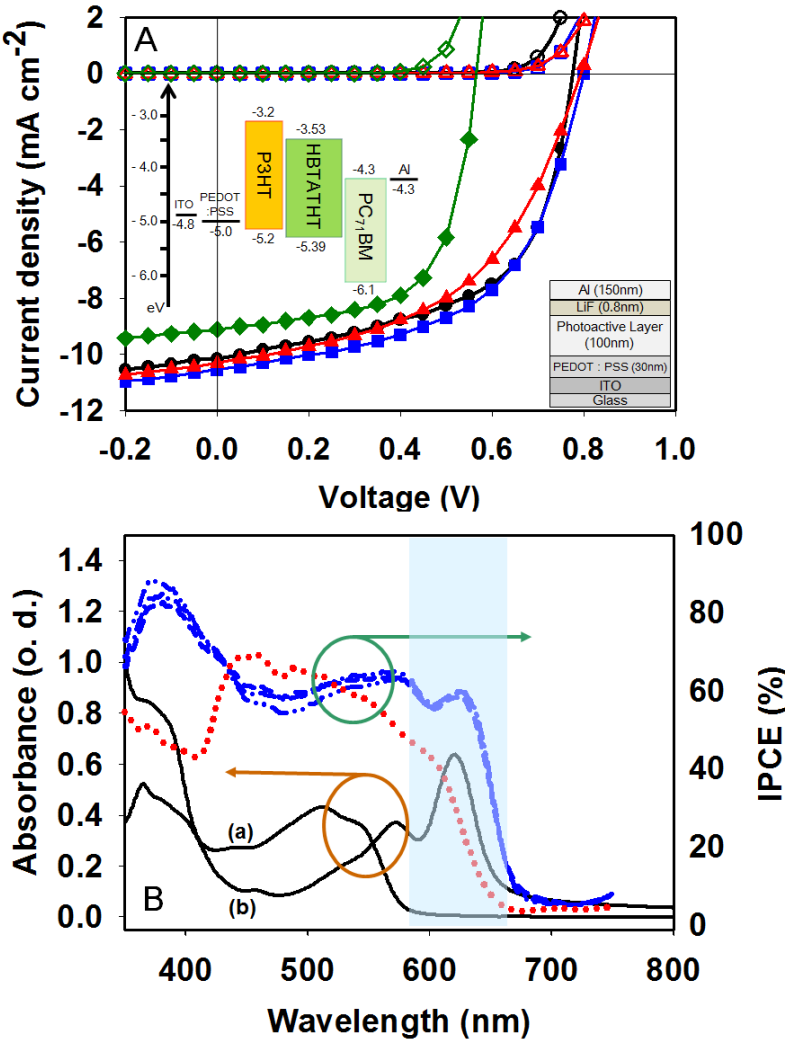

Figure 12S. (A) *J-V* characteristics of OPVs based on **HBTATHT** : $PC_{71}BM$ active layer with various blend compositions. *open symbols: dark current, filled symbols: photocurrent under AM 1.5 white light illumination at 100 mW cm^{-2}, *circle (1:0.8), square (1:0.6), triangle (1:0.4), diamond (P3HT:$PC_{71}BM$ =1:0.6) (B) External quantum efficiency (EQE) of OPV cells with **HBTATHT** : $PC_{71}BM$ active layer with different blend composition. *Medium dashed line (1:0.8), Dash-dot-dashed line (1:0.6), Dash-dot-dot-dashed line (1:0.4), dotted line (P3HT:$PC_{71}BM$=1:0.6). *The absorption spectra of **HBTATHT** were superimposed. (a) solution, (b) film. *The shaded area denotes enhancement of absorption and EQE due to J-aggregation of **HBTATHT** compared to those of P3HT/$PC_{61}BM$ system.

16. AFM and TEM images of the blend films of HBTATHT and $PC_{61}BM$.

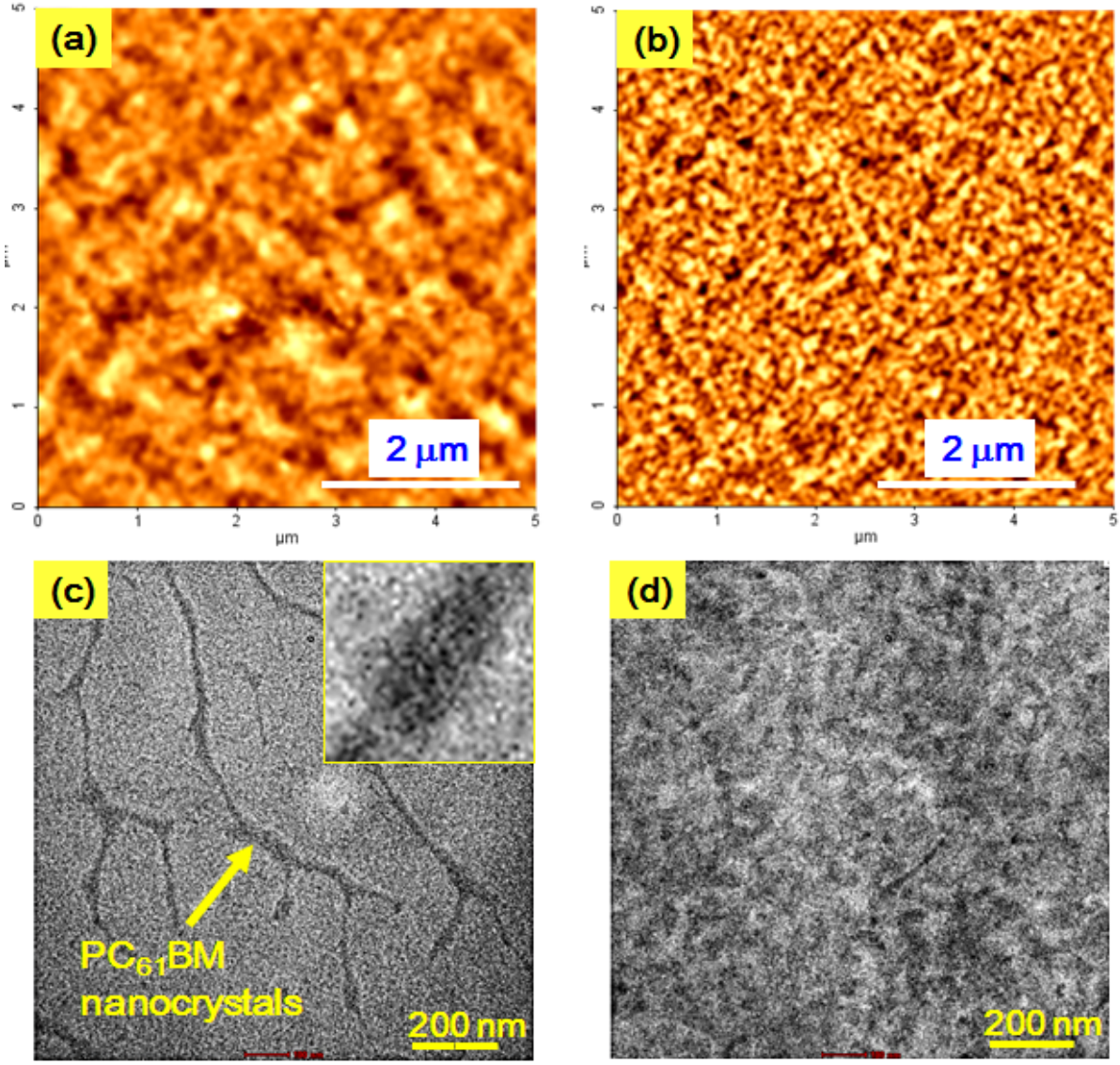

Figure 13S. AFM (a, b) and TEM (c, d) images of photoactive layer prepared from CB solvent in OPV devices.; (a) and (c) **HBTATHT**: $PC_{61}BM$ (1: 0.8, η= 4.84 %), (b) and (d) **HBTATHT**: $PC_{61}BM$ (1: 1, η= 3.85 %).

17. AFM and TEM images of the blend films of HBTATHT and $PC_{71}BM$.

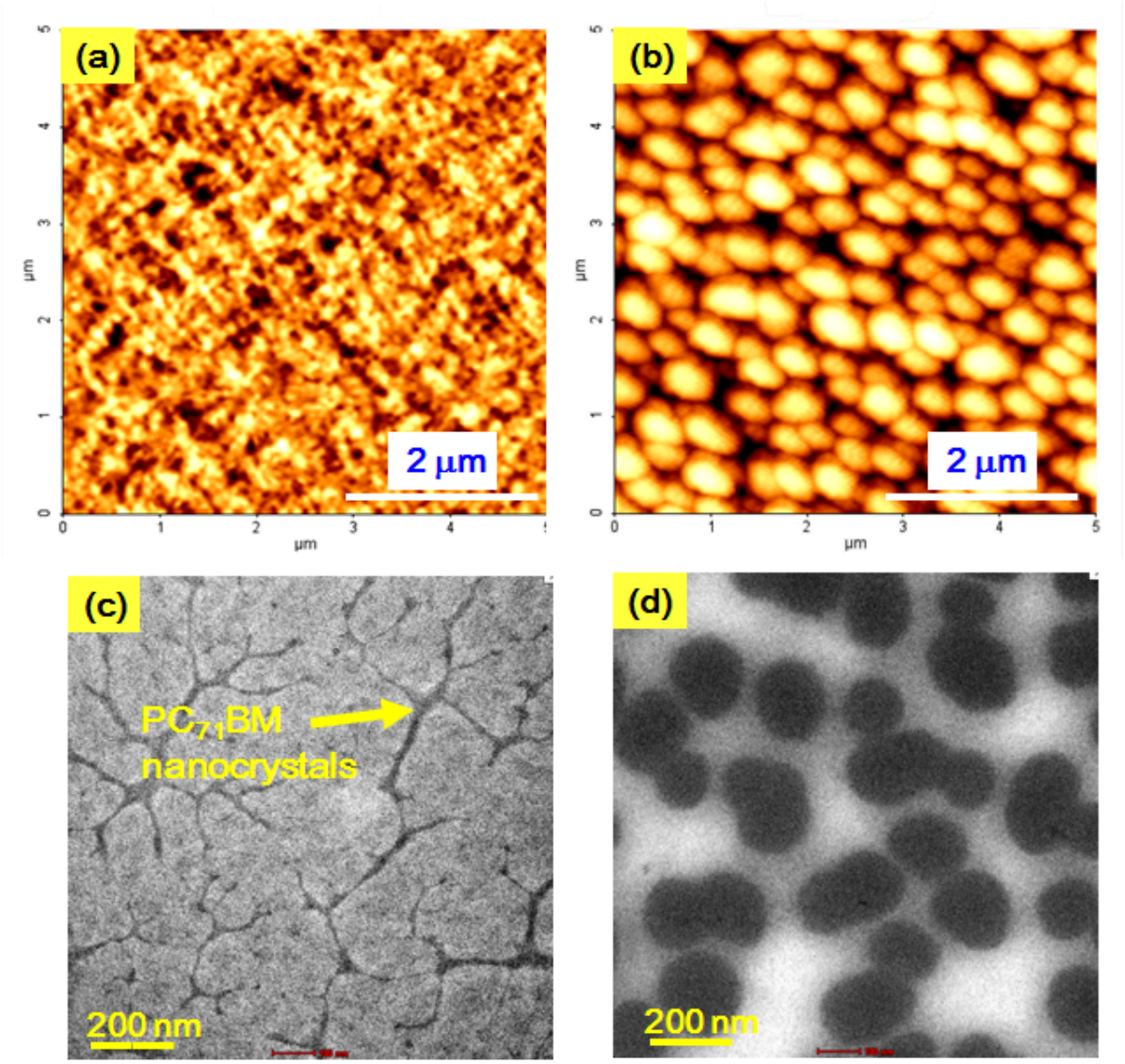

Figure 14S. AFM (a, b) and TEM (c, d) images of photoactive layer prepared from CB solvent in OPV devices.; (a) and (c) **HBTATHT**: $PC_{71}BM$ (1: 0.6, η= 4.70 %), (b) and (d) **HBTATHT**: $PC_{71}BM$ (1: 2, η= 1.62 %).

18. Device performances of BHJ PV devices based on HBTATHT : PCBM.

Table 1S. Device properties of OPVs based on **HBTATHT** : PCBM.

HBTATHT:PCBM wt. ratio	J_{sc} (mA cm^{-2})	V_{oc} (V)	FF	PCE (%)
1 : 4 [a]	-3.92	0.81	0.48	1.52
1 : 2 [a]	-6.38	0.79	0.47	2.37
1 : 1 [a]	-8.91	0.79	0.54	3.85
1 : 0.8 [a]	-10.00	0.81	0.59	4.84
1 : 0.6 [a]	-9.83	0.81	0.55	4.43
1 : 4 [b]	-4.31	-0.69	0.48	1.44
1 : 2 [b]	-4.75	0.67	0.50	1.62
1 : 0.8 [b]	-10.15	0.79	0.57	4.63
1 : 0.6 [b]	-10.59	0.80	0.55	4.70
1 : 0.4 [b]	-10.31	0.79	0.50	4.12
1 : 0.6[c]	-9.20	0.57	0.64	3.39

[a] acceptor, $PC_{61}BM$; [b] acceptor, $PC_{71}BM$; [c] P3HT:$PC_{61}BM$

19. References

[S1] K. H. Kim, S. Y. Bae, Y. S. Kim, J. A. Hur, M. H. Hoang, T. W. Lee, M. J. Cho, Y. Kim, M. Kim, J.-I. Jin, S.-J. Kim, K. Lee, S. J. Lee, D. H. Choi, *Adv. Mater.,* 2011, **23**, 3095.

[S2] J. A. Hur, S. J. Kim, K. H. Kim, T. W. Lee, K.-H. Kim, J. Shin, K. S. Hwang, B. D. Chin, D. H. Choi, *Synth. Met.,* 2012, **161**, 2776.

[S3] S. Y. Bae, S. Y. Jo, K. H. Kim, T. W. Lee, D. H. Choi, *Mol. Cryst. Liq. Cryst.,* 2011, **538**, 175.

[S4] S. Y. Jo, J. Shin, S. Y. Bae, K. H. Kim, T. W. Lee, S.-H. Son, K.-K. Kim, D. H. Choi, *Synth. Met.,* 2011, **161**, 833.

[S5] J. A. Hur, S. Y. Bae, K. H. Kim, T. W. Lee, M. J. Cho, D. H. Choi, *Org. Lett.,* 2011, **13**, 1948.

[S6] S. Y. Bae, K. H. Jung, M. H. Hoang, K. H. Kim, T. W. Lee, M. J. Cho, J.-I. Jin, D. H. Lee, D. S. Chung, C. E. Park, D. H. Choi, *Synth. Met.,* 2010, **160**, 1022.

[S7] K. H. Jung, S. Y. Bae, K. H. Kim, M. J. Cho, K.-Y. Lee, Z. H. Kim, D. H. Choi, D. H. Lee, D. S. Chung, C. E. Park, *Chem. Commun.,* 2009, **35**, 5290.